CFD Simulation and Investigation of Slurry Flows in Pipelines

Marwane ElKarii

Mines ParisTech, CES, Paris, France

Mohammed VI Polytechnic University (UM6P), MSDA, Ben Guerir, Morocco

Octorber 2021

Contents

Chapter 1

Introduction

Pipeline transport of solid-liquid sludge is an essential operation in many areas, such as mining and chemical processing. This comes down to the fact that pipelines are more efficient and environmentally friendly than railway transportation. Yet, the transported fluid may be highly viscous and have complex rheology. Moreover, the flow within the pipe is generally highly turbulent and complex (Lahiri and Ghanta [2010]) and problems like pipe plugging, and solid sedimentation could occur. Therefore, to ensure a continuous and optimal flow, different parameters should be controlled. In particular, the distribution of solids and the pressure drop within the pipeline represent a serious concerns to engineers, since their determination involves considerable technical difficulties. Thus, having means to predict the physics of the slurry flow is essential for the control of the pipeline process. The rapid increase in computational power has made it possible to widely distribute different tools and techniques, capable of modeling complex flows in real-dimensional geometries. This paved for a better handling of such flows by complementing empirical methods with digital simulations. Therefore, Computational Fluid Dynamics (CFD) has appeared as an effective tool to model and predict unknown or particular slurry flow scenarios (Bin and DaWen [2002]), and it can provide a series of monitoring information, which is difficult to achieve by experience alone. The advantages of CFD can be categorized as

- It provides a detailed understanding of flow distribution, mass and heat transfer, particulate separation, etc. Consequently, all these will lead to a much better and deeper understanding of what is happening in a particular process or system.

- It is able to reduce scale-up problems because the models are based on fundamental physics and are scale independent.
- It is particularly useful in simulating conditions where it is not possible to take detailed measurements.

1.1 CFD approaches for multiphase flows

Generally, the CFD approaches for the simulation of slurry flows can be classified into:

- Eulerian-Lagrangian approaches (Crowe et al. [2011]), where the liquid phase is modeled as a continuum and solved in an Eulerian cell-based framework, whereas the behavior of the solid phase is obtained by the Discrete Particle Method (DPM), in which the individual trajectories of computational particles are calculated in a Lagrangian fashion.
- Eulerian-Eulerian approaches (Crowe et al. [2011]), where both phases are modeled as interpenetrating continua, and two sets of conservation equations are solved jointly in the Eulerian framework. The coupling between the two phases depends on the amount of solids in the flow, and it ranges from one-way coupling for dilute slurries (*i.e.*, the particles do not affect the liquid flow field) to four-way coupling for dense slurries (where the particle-particle and particle-fluid interactions are important as well). This approach characterizes the majority of the earlier CFD investigations of slurry pipe flows which provides a good compromise between accuracy and computational cost. Yet three models are possible within this approach.

Table 1.1 shows a comparison of the latter models. [1]

Table 1.1: Comparison between Euler-Euler models

VOF	Mixture Model	Multi-phase Eulerian Model
Modelling non-miscible fluid	Model used if there is a wide distribution of dispersed phases	Interphase laws available.
A single set of motion equations	Interphase laws not available	More precise.
Examples: free surface flow (Jing et al. [2016])), large bubbles in a liquid (Al-Yaari and Abu-Sharkh [2011])), stratified flow (Akhtar et al. [2007]))	Examples: particle-laden flow* with low load (Dufek and Bergantz [2007]), bubble flow, sludge flow (Chen et al. [2009])	Examples: sludge flow (Ofei and Ismail [2016]), sedimentation ((Gopaliya and Kaushal [2016]), fluidized beds (Ofei et al. [2014])).

1.2 Problem Description

This work concerns the transport of phosphate ores in the context of an industry 4.0. The process begins with the extraction of ore that is transported as pulp (Water + Phosphate) in a pipe (pipeline), from the mine to the industrial units for processing (cf. Fig. 1.1). This

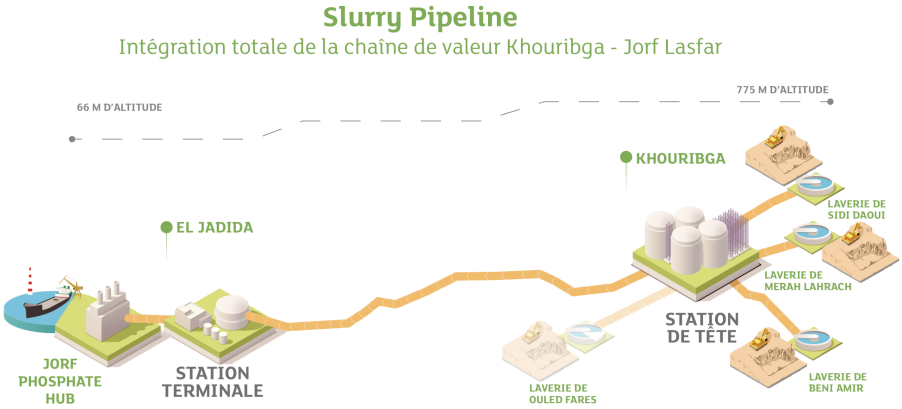

Figure 1.1: Transport process of phosphate slurry

pulp is characterized by a solid volume concentration that goes up to 40 %, it contains rigid solid particles of random shapes having an equivalent spherical diameter ranging from 44 μm to 400 μm. The ore particles are characterized by an average total porosity of 20 % by volume, then an effective density of 2600 kg/m^3 when the pores are filled with water. The operation of the phosphate slurry pipe is controlled by a series of pressure and choke stations. The pipeline receives the phosphate ore, of different qualities, from four different washing stations, which gives it variable flow properties (viscosity, density, speed, pressure...). The phosphate pulp is transported in batches, separated by batches of water to control the quality and flow of the pulp (cf. Fig. 1.2).

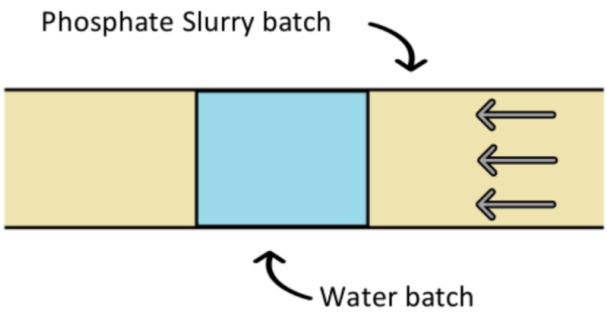

Figure 1.2: Phosphate slurry flow

[1] Particle-laden flow = Particle charge flows refer to a two-phase flow in which one of the phases is continuously connected and the other phase consists of small immiscible particles and typically diluted.

The main challenge of the work to be carried out in the context of this thesis is is to set the basis for an intelligent control for the transport process, based on computational fluid dynamics (CFD) simulation models. This system will ensure optimal operation of the process, predict the evolution of certain critical parameters and contribute to operational decision-making. From an application point of view, among the industrial stakes of the project of this thesis:

- Increase productivity (volume sent by the pipe);
- Secure the pipe by mastering the characteristics of the pulp;
- Predict solid concentration profiles and pressure losses in the pipeline;
- Optimize pipe operation according to pulp quality;
- Optimize energy consumption, etc;

Chapter 2

Literature Review : slurry pipes modeling and simulation

A summary of the most relevant numerical studies on slurry flows in horizontal pipes published so far are reported, alongside with the adopted modelling approach. Beginning with Eulerian-Lagrangian approach, this latter was employed for this kind of applications for sand-water slurry by Cap, where the Large Eddy Simulation (LES) method Versteeg and Malalasekera [2007] has been used to simulate the turbulent flow of the liquid phase, while the solid phase was treated by DPM. ARO [2015] used the same numerical setup to characterize a sand-water flow pattern for increasing values of liquid superficial velocity. Always in the Eulerian-Lagrangian approach but this time it was employed with different characteristics such as transportation of coarse NaCl particles in brine by Uzi, where the liquid phase is handled by a computationally cheaper Reynolds-Average Navier-Stokes (RANS) technique, to examine the effects of the operating conditions on the flow. Concerning the mixture model, J-2 performed CFD simulations for sand-water slurry flows through horizontal pipes, where a simplified 3D algebraic slip mixture (ASM) model is introduced along with RNG k–ϵ turbulent model to obtain the precise numerical solution in fully developed turbulent flow. They compared CFD results of mean pressure gradients with experimental results, and found a big discrepancy between them takes place when the mean velocities of slurry flows are lower than corresponding critical deposition velocities. C.X numerically investigated sand–water slurry flows in the entrance region of horizontal pipe, again using ASM model, and have focused mainly on illustrating and comparing the developing processes of various flow parameters. Sil performed simulations for Saline Water-Glass beads

slurry using Mixture Model coupled with a High Reynolds k–ϵ turbulence model, results were validated with data attained with an Electrical tomography apparatus. The model produced accurate representations for the highest flow rates, while showing some deviations for the lower flow rate. However, the majority of the earlier CFD investigations of slurry pipe flows were performed using the Two Fluid Model. In most TFMs, constitutive equations for the solid phase derived from the Kinetic Theory of Granular Flow (KTGF) were employed. The most relevant numerical studies on slurry flows in horizontal pipes published so far, the study of Hernandez et al. [2008] for sand-water slurry, where homogeneous and heterogeneous flow regimes without bed were considered along with predictions of pressure gradients at the fully developed zone. Eka investigated the effect of in situ solids volume concentration, particle size, mixture velocity, and pipe diameter, on local time-averaged solids concentration profiles, particle and liquid velocity profiles, and frictional pressure loss. Excellent agreement between the predicted and the experimental was obtained. Chen et al. [2009] used the same numerical configuration to simulate flow of coal-water slurries (CWS) in a horizontal pipeline, with bimodal distribution for coal particles. They found out that the simulation results of the binary solid phase model is closer to experimental data, as compared to the results of the single solid phase model. Bossio et al. [2009] focused on modeling of non-Newtonian Laterite-Sand slurry where the mean pressure gradients were compared with experimental data. Antaya et al. [2012] performed simulations for concentrated mixtures of sand-water slurry with mono-sized and bimodal particle sizes. Shear stress model (SST) was tested in addition to the k–ϵ model to treat the turbulence of the continuous phase. Success has been achieved in the use of k–ϵ model, with the SST model being superior, especially in the near-wall region. However D.R, tried both Mixture and two-phase model to simulate mono-dispersed fine particles at high concentration of glass beads mixed with water. They proved again the failure of the Mixture Model predictions at high velocities and high solid concentrations compared to TFM. Y.Y worked on an unusual type of slurry flows which is Slush nitrogen flow using the 2D Eulerian – Eulerian multiphase approach. The per-phase k–ϵ turbulence model is used in the study to model the turbulent two-phase flow. The effects of the flow velocity and the mean solid volume fraction on the flow characteristics of slush nitrogen are investigated numerically in this study. The same team in very next year Jia investigated the same slush and nitrogen flow. Based on the experimental and numerical results they distinguished three flow patterns, which for each one they had studied the variation of pressure drop. They obtained the general correlation of the friction factor with the slush

Reynolds number of slush nitrogen with various solid volume fractions. Wan applied the two fluid model to describe an ice slurry flow without considering ice melting. After validation of the model with experimental data, it was used to investigate the distributions of ice slurry flow, ice particle concentration and pressure drop in horizontal, vertical and 90 elbow pipes respectively. They found that for pressure drop, the numerical model is found being able to provide results in good agreement with the experimental data where the relative errors are limited to 20%. Mes [a] developed a new two-fluid model for the simulation of Sand and Glass beads Water slurry. Contrary to previous works with TFM models, they did not integrate the kinetic theory of granular flows to determine solid viscosity. They studied the effect of the wall boundary condition for the solid phase on the pressure gradient, where they found that the best match between measurements and computations is obtained when the equilibrium logarithmic law of Launder and Spalding for smooth walls is applied to the solid phase. Then, Mes [b] used the new TFM model to simulate a fully-suspended Sand-Water slurry flow in horizontal pipes and bends. They claimed that the model is robust and numerically stable, and requires relatively short computer time to provide a converged steady-state solution. The novelty of the proposed model and its better performance compared to similar ones reside in the method of accounting for some key physical mechanisms governing these flows, namely turbulent dispersion, interphase friction, and viscous and mechanical contributions to friction. Mes [c] further modified Mes [b] model by incorporating a new wall boundary condition for the solid phase, a more general correlation for the viscosity of the slurry, accounting for particle shape along with a different solution algorithm. These changes resulted in low computational effort with improved performance. They verified the modified model by comparing its outcomes with experimental results for sand-water slurries available in the literature. returning to the TFM combined with KTGF, Gop studied the effects of grain size on various Sand-Water slurry flow parameters. They found that at the same volumetric concentration, pressure drop increases with increase in grain size. Has performed experiments in a 265 mm diameter pipe loop with sand-in-water slurries, then selected experimental conditions were numerically simulated using a commercial CFD package, ANSYS CFX. They noticed that the agreement between the numerical results and the experimental data is concentration dependent, with relatively closer agreement at lower concentrations. Kumar et al. [2017] presented experimental data of iron-ore slurry flow cases through 105 mm pipe, the obtained results are validated using TFM-KTGF model. Results reflect good resemblance between measured and predicted pressure drops, solid concentrations

and velocity profiles. Singh et al. [2017] investigated the flow characteristics of coal water slurry having high solid concentrations in slurry pipeline. They have noticed that the coal-water slurry shows Newtonian behaviour at 30% solid concentration (by-weight) and beyond this it depicts non Newtonian pseudo plastic behavior. In this study also SST k-ω turbulence model was found a better predictor over other models namely Standard k-ϵ, RNG k-ϵ, Realizable k-ϵ and Standard k-ω models. A year after Li- [a] developed a useful three-dimensional multiphase hydrodynamic model based on the kinetic theory of granular flow, for simulating multi-sized glass beads-water slurry transport through pipelines, to investigate the distributions of solid concentration, flow velocity, granular pressure, and wall shear stress. The simulation result of different-sized particle behaviors in multi-sized slurry has significant reference value. Li- [b] also in the same year studied the effect of interaction of particles with different sizes on particle kinetics in multi-sized slurry, first They concluded that the speed of resistance increase in a graded slurry is more gradual than in a single-sized slurry with the same conditions as the solid concentration increases,then they found that the wall shear stress of coarse particles is significantly reduced by the existence of fine particles with increasing flow rate and solid concentration, and finally they affirmed that the existence of fine particles significantly reduces the collision intensity of coarse particles and velocity fluctuations in the multi-sized slurry. Recently, Mes [d] considered again the same Two Fluid Model, but this time for a deeper physical interpretation, and to provide recommendations of general validity. For the sake of generality and strength of the numerical model, three different data sets were considered for the experimental verification of the model, resulting in 108 different simulation scenarios covering a wide range of pipe diameters, solid concentrations, and slurry velocities.

Summary on models classification

Following the literature review presented above, our CFD approach will be based on the Eulerian model (Two Fluid Model) as it is the most complete model and the most used one to deal with suspensions transport issues, and is confirmed to be the most accurate and gives generally good results. While mixture model fails to predict pressure drops correctly and the amount of error increases rapidly with the slurry concentration (D.R). The main conclusions from the literature review are summed in table 2. The description of the TFM model is given in section 3.1. The dynamics of the solid phase is modeled by the KTGF to consider both particle collisions and frictions. Also, based on the previously cited works, the turbulence of the continuous phase is

treated by the k-ϵ based models, that generally shows reasonable robustness, and give reasonable accuracy for a wide range of applications. Yet, even though success is usually achieved using models based on the k-epsilon, it should be made clear that they may not perform well in the region near the wall (Antaya et al. [2012]). Therefore, a near-wall treatment model is presented in section 3.4, to address the weak performance of the choosed turbulence models in this area of the pipe.

Table 2.1: Summary on models classification

Models	Conclusions
DPM (Eulerian-Lagrangian Approach)	The discrete phase must be present at a fairly low volume fraction, usually less than 10-12%
Mixture Model	There is a big discrepancy between CFD results with experimental, especially at lower flow rates.
TFM Model	TFM is accurate and gives generally good results comparing to the mixture model. TFM results are better and closer to the experimental data in the case of bimodal particle sizes or at higher velocities.

In fact, modern modeling strategies, for industrial processes, integrates usually 3D simulation techniques using computational fluid dynamics (CFD) and/or discrete element methods (DEM). These 3D models are then integrated as surrogate models that can be used in operations simulation and monitoring tools (Decision Support Systems). Classically, response surface methodologies (RSM) are applied to build a polynomial surrogate model (Rabhi et al. [2018]), but also in recent works machine leaning techniques such as artificial neural networks (ANN) can be used (Seong et al. [2020]). The current modeling approach consists of constructing 3D models for different type of pipe elements (horizontal, inclined, bended pipes), and then use them to construct surrogates that models the pressure drop within each element. Such models can then be used in dynamical models for monitoring slurry pipe systems and to conduct sizing studies to cover variations in the operation conditions like inlet pressure and inlet flow rate. This approach will first be applied to a single fluid flow to validate the approach of constructing a surrogate pressure drop model through 3D numerical simulation, and then to slurry flows with solid volume fraction up to 25%.

A parametric analysis is conducted to investigate the impact of the variation in the particle

size, solids concentration, and inlet velocity, on the solid concentration profile, the solid velocity profile and finally their effect on the variation in the pressure drop along the pipe. This analysis allows us to validates our simulations for turbulent slurry flows versus experimental data. The data used in this work is regarding a horizontal pipe case for Water-Sand slurry flow: transported solid volume fraction between 19 % and 45 %; velocities between 1 m/s and 8.0 m/s; and particles sizes of 90 μ_m and 270 μ_m.

Chapter 3

Theoretical and empirical models

3.1 Mathematical models

In the two-fluid Eulerian-Eulerian approach, each phase is described by a set of averaged conservation equations. The present formulation follows Elkarii et al. [2020], Passalacqua and Fox [2011]. A general discussion of how such models are derived via averaging can be found in Drew and Passman [2006]. Introducing the particle volume fraction field ϕ, the governing equations for the two phases are expressed as follows

$$\begin{cases} \partial_t \left(\varrho_\mathfrak{f} \phi_\mathfrak{f} \right) + \partial_i \left(\varrho_\mathfrak{f} \mathrm{u}_{\mathfrak{p},i} \phi_\mathfrak{f} \right) = 0, \\ \varrho_\mathfrak{f} \phi_\mathfrak{f} \left(\partial_t \mathrm{u}_{\mathfrak{f},i} + \mathrm{u}_{\mathfrak{f},j} \partial_j \mathrm{u}_{\mathfrak{f},i} \right) = \varrho_\mathfrak{f} \phi_\mathfrak{f} g_i - \phi_\mathfrak{f} \partial_i \mathfrak{p} + \partial_j \tau_{\mathfrak{f},ij} + \mathrm{F}_{\mathfrak{f},i}, \end{cases} \tag{3.1}$$

where the letter t represents the time and the symbols ∂_t and ∂_i denote the partial differential operators ∂/∂_t and $\partial/\partial x_i$, respectively. Furthermore, the summation convention for repeated indices is used. Here, $\phi_\mathfrak{f}$ is the volume fraction and $\varrho_\mathfrak{f}$ the density of the respective fluid. The velocity vector is denoted by $\mathbf{u}_\mathfrak{f}$, the pressure by $\mathfrak{p}$, and the gravity by $\boldsymbol{g}$. The index $\mathfrak{f}$ is symbolic for the solid and the fluid phase, e.g. the solid phase fraction may be denoted by $\phi_\mathfrak{p}$, the one of the continuous phase as $\phi_\mathfrak{w}$. The sum of the volume fraction of the different phases is always unity. The stress tensor is evaluated as $\tau_{\mathfrak{f},ij} = 2\phi_\mathfrak{f}\mu_\mathfrak{f}\left(\mathcal{S}_{\mathfrak{f},ij} - \mathcal{S}_{\mathfrak{f},kk}\delta_{ij}/3\right)$ with $\mathcal{S}_{ij} = \left(\partial_j \mathrm{u}_{\mathfrak{f},i} + \partial_i \mathrm{u}_{\mathfrak{f},j}\right)/2$. The last term $\mathbf{F}_\mathfrak{f}$ in (3.1) denotes the momentum transfer between the phases. It is decomposed into drag forces $\mathbf{F}^{\mathrm{d}}_\mathfrak{f}$, lift forces $\mathbf{F}^{\mathrm{l}}_\mathfrak{f}$, and turbulent dispersion forces

$\mathbf{F}_{\mathfrak{f}}^{\mathrm{vm}}$ and it is expressed therefore as

$$\mathbf{F}_{\mathfrak{f},i} = \mathbf{F}_{\mathfrak{f}}^{\mathrm{d}} + \mathbf{F}_{\mathfrak{f}}^{\mathrm{l}} + \mathbf{F}_{\mathfrak{f}}^{\mathrm{vm}}. \tag{3.2}$$

In the present two-fluid calculation, the following functional forms Maxey and Riley [1983] are retained

$$\begin{cases} \mathbf{F}_{\mathfrak{f}}^{\mathrm{d}} = \frac{3}{4}\frac{\varrho_{\mathfrak{w}}}{\mathrm{d}_{\mathfrak{s}}}\mathcal{C}_{\mathrm{d}}\|\mathbf{u}_{\mathfrak{w}} - \mathbf{u}_{\mathfrak{s}}\|\left(\mathbf{u}_{\mathfrak{w}} - \mathbf{u}_{\mathfrak{s}}\right), \\ \mathbf{F}_{\mathfrak{f}}^{\mathrm{l}} = \varrho_{\mathfrak{w}}\mathcal{C}_{\mathrm{l}}(\mathbf{u}_{\mathfrak{w}} - \mathbf{u}_{\mathfrak{s}}) \times (\nabla \times \mathbf{u}_{\mathfrak{w}}), \\ \mathbf{F}_{\mathfrak{f}}^{\mathrm{vm}} = \varrho_{\mathfrak{w}}\mathcal{C}_{\mathrm{vm}}\left(\mathrm{D}_t^{\mathfrak{w}}\mathbf{u}_{\mathfrak{w}} - \mathrm{D}_t^{\mathfrak{s}}\mathbf{u}_{\mathfrak{s}}\right), \end{cases} \tag{3.3}$$

where $\mathrm{D}_t^{\mathfrak{f}} = \partial_t + \mathrm{u}_{\mathfrak{f},j}\partial_i$ stands for the substantive derivative corresponding to each phase $\mathfrak{f}$, and $\mathcal{C}_{\mathrm{d}}$, $\mathcal{C}_{\mathrm{l}}$ and $\mathcal{C}_{\mathrm{vm}}$ are the drag, lift and virtual mass coefficients, respectively. For the drag coefficient, the solid particle drag model of Wen and Yu [1966] is retained, which reads

$$\mathcal{C}_{\mathrm{d}} = \begin{cases} \frac{24}{\mathcal{R}\mathfrak{e}}\left(1 + 0.15\mathcal{R}\mathfrak{e}^{0.687}\right)\left(1 - \phi_{\mathfrak{s}}\right)^{-2.7} & \text{, if } \mathcal{R}\mathfrak{e} \leq 10^3, \\ 0.44\left(1 - \phi_{\mathfrak{s}}\right)^{-2.7} & \text{, if } \mathcal{R}\mathfrak{e} \geq 10^3, \end{cases} \tag{3.4}$$

where $\mathcal{R}\mathfrak{e} = \varrho_{\mathfrak{s}}\|\mathrm{u}_{\mathfrak{r}}\|\mathrm{d}_{\mathfrak{s}}/\mu_{\mathfrak{s}}$ is the Reynolds number bases on the particle diameter $\mathrm{d}_{\mathfrak{s}}$ and the relative velocity $\mathbf{u}_{\mathfrak{r}} = \mathbf{u}_{\mathfrak{w}} - \mathbf{u}_{\mathfrak{s}}$. For virtual mass coefficient $\mathcal{C}_{\mathrm{d}}$, a fixed value of 0.5 is used throughout the present study Auton et al. [1988].

The solid phase is modelled in this Eulerian framework as an interpenetrating fluid but with a viscosity that is determined by the kinetic theory of granular flows

Solid-phase viscosity

Solid-phase viscosity is determined using Kinetic Theory of Granular flows(KTFG) which is based on the kinetic theory of gases in a generalized way to take into account collisions of inelastic particles to define a granular temperature θ in solid phase which directly affects the phase stress tensor (Gon). Analogical to the thermodynamic temperature for gases, the granular temperature $\Theta = \frac{1}{3} < v_s'^2 >$ was introduced as a measure for the energy of the fluctuating velocity of the particles Lun et al. 1987. The equation of conservation of solids fluctuating energy can be expressed as Wan:

$$\frac{3}{2}\left[\frac{\partial}{\partial t}\left(\alpha_s \rho_s \Theta_s\right) + \nabla \cdot \left(\alpha_s \rho_s \mathbf{u}_s \Theta_s\right)\right] = \underbrace{\left(-P_s \mathbf{I} + \tau_s\right) : \nabla \mathbf{u}_s}_{\text{Production due to shear stress}} + \underbrace{\nabla \cdot \left(\kappa_\Theta \nabla \Theta\right)}_{\text{Diffusion}} \tag{3.5}$$

$$- \underbrace{\gamma_{\Theta_S}}_{\text{Dissipation due to inelastic collisions}} + \underbrace{\Phi_{LS}}_{\text{Dissipation/Production due to the interaction with the carrier}}$$

Rather than solving the complete granular energy balance given in Equation 1, Eka assume the granular energy is in a steady state and dissipated locally and neglect convection and diffusion. Retaining only the generation and the dissipation terms, Equation 1 simplifies to an algebraic expression for the granular temperature:

$$\left(-p_\mathrm{s} \overrightarrow{\mathrm{I}} + \vec{\tau}_\mathrm{s}\right) : \vec{\nabla} \vec{u}_\mathrm{s} - \gamma_{\Theta \mathrm{s}} + \Phi_{LS} = 0 \tag{3.6}$$

Expression for all the terms can be derived (GID):

$$\gamma_{\Theta_\mathrm{S}} = \frac{12\left(1 - e^2\right) g_0}{d_\mathrm{S} \sqrt{\pi}} \rho_\mathrm{S} \alpha_\mathrm{S}^2 \Theta_\mathrm{S}^{3/2} \tag{3.7}$$

$$\phi_{\mathrm{LS}} = -3 \mathrm{K}_{\mathrm{SL}} \Theta_\mathrm{S} \tag{3.8}$$

$$p_\mathrm{S} = \alpha_\mathrm{S} \rho_\mathrm{S} \Theta_\mathrm{S} + 2 \rho_\mathrm{S}\left(1 + e\right) \alpha_\mathrm{S}^2 g_0 \Theta_\mathrm{S}\right) \tag{3.9}$$

where e is the coefficient of restitution for particle collisions that quantifies the elasticity of particle collisions. (g_0) is the radial distribution function that can also be seen as a probability for interaction between particles. Different models exists, they are formulated is in table 2. The solid bulk viscosity λ_S accounts for the granular particles resistance of compression and expansion. It can be calculated by the following form (Eka):

$$\lambda_\mathrm{S} = \frac{4}{3} \alpha_\mathrm{S} \rho_\mathrm{S} d_\mathrm{S} g_0 \left(1 + e\right) \left(\frac{\Theta_\mathrm{S}}{\pi}\right)^{\frac{1}{2}} \tag{3.10}$$

Then, the solid shear viscosity μ_S based on granular kinetic theory consists of a collisional contribution and from a kinetic contribution. It can be represented as (GID):

$$\mu_\mathrm{S} = \mu_{\mathrm{S,col}} + \mu_{\mathrm{S,kin}} \tag{3.11}$$

Table 2 show different Kinetic Theory Correlations for μ_S and g_0.

Table 3.1: Kinetic Theory Correlations

	Granular viscosity μ_s
Lun et al. [1984]	$\frac{4}{5}\alpha_s^2\rho_s d_s g_0(1+e)\sqrt{\frac{\Theta}{\pi}} + \frac{1}{15}\sqrt{\Theta\pi}\frac{\rho_s d_s g_0(1+e)\left(\frac{3}{2}e-\frac{1}{2}\right)\alpha_s^2}{\frac{3}{2}-\frac{1}{2}e} + \frac{1}{6}\sqrt{\Theta\pi}\frac{\rho_s d_s \alpha_s\left(\frac{s}{2}e+\frac{1}{4}\right)}{\frac{3}{2}-\frac{e}{2}} + \frac{10}{96}\sqrt{\Theta\pi}\frac{\rho_s d_s}{(1+e)\left(\frac{3}{2}-\frac{1}{2}e\right)g_0}$
Syamlal et al.	$\frac{4}{5}\alpha_s^2\rho_s d_s g_0(1+e)\sqrt{\frac{\Theta}{\pi}} + \frac{1}{15}\sqrt{\Theta\pi}\rho_s d_s g_0\frac{(1+e)\left(\frac{3}{2}e-\frac{1}{2}\right)}{\frac{3}{2}-\frac{e}{2}}\alpha_s^2 + \frac{1}{12}\frac{\alpha_s d_s \rho_s\sqrt{\pi\Theta}}{\frac{3}{2}-\frac{e}{2}}$
GID	$\frac{4}{5}\alpha_s^2\rho_s d_s g_0(1+e)\sqrt{\frac{\Theta}{\pi}} + \frac{1}{15}\sqrt{\Theta\pi}\rho_s d_s g_0(1+e)\alpha_s^2 + \frac{1}{6}\sqrt{\Theta\pi}\rho_s d_s\alpha_s + \frac{10}{96}\sqrt{\Theta\pi}\frac{\rho_s d_s}{(1+e)g_0}$
hen	$\frac{4}{5}\epsilon_s^2\rho_s d_s g_0(1+e)\sqrt{\frac{\Theta}{\pi}} + \frac{1}{15}\sqrt{\Theta\pi}\frac{\rho_s d_s g_0(1+e)\left(\frac{3}{2}e-\frac{1}{2}\right)\epsilon_s^2}{\left(\frac{3}{2}-\frac{c}{2}\right)} + \frac{1}{6}\sqrt{\Theta\pi}\frac{\rho_s d_s \epsilon_s\left(\frac{1}{2}\left(1+\frac{\lambda_m f_p}{R}\right)+\frac{3}{4}e-\frac{1}{4}\right)}{\left(\frac{3}{2}-\frac{1}{2}e\right)\left(1+\frac{\lambda_m(p)}{R}\right)} + \frac{10}{96}\sqrt{\Theta\pi}\frac{\rho_s d_s}{(1+e)\left(\frac{3}{2}-\frac{1}{2}e\right)g_0\left(1+\frac{\lambda_m f_p}{R}\right)}$
	Radial Function g_0
Car	$\frac{1}{1-\epsilon_s}+\frac{3\epsilon_s}{2(1-\epsilon_s)^2}+\frac{\epsilon_s^2}{2(1-\epsilon_s)^3}$
Lun and Savage [1986]	$\left(1-\frac{\alpha_s}{\alpha_{s,\max}}\right)^{-2.65\alpha_{s,\max}}$
sin	$\left[1-\left(\frac{\alpha_s}{\alpha_{s,\max}}\right)^{\frac{1}{3}}\right]^{-1}$
GID	$\frac{3}{5}\left[1-\left(\frac{\alpha_s}{\alpha_{s,\max}}\right)^{\frac{1}{3}}\right]^{-1}$

Remarks:

For granular viscosity:

- hen follow Lun et al. [1984] but constrain the mean free path of the particle by a dimension characteristic of the actual physical system. This is opposed to the Lun et al. [1984] theory which allows the mean free path to tend toward infinity.
- Lun et al. [1984] theory which allows the mean free path to tend toward infinity and the solids viscosities tends toward a finite value as the solids volume fraction tends to zero.
- By constraining the mean free path, the limit of the hen shear viscosity expression correctly tends to zero as the solids volume fraction approaches zero.
- Syamlal et al. solids shear viscosity also tends to zero as the solids volume fraction tends to zero. In this case, however, the solids shear viscosity limit is reached because the kinetic contribution to the solids viscosity is neglected.

For radial function:

- The Car expression, however, does not tend toward the correct limit at closest solids packing. Because particles are in constant contact at the maximum solid volume fraction, the radial distribution function at contact tends to infinity.
- Alternate expressions to the Car expression have been proposed by GID, Lun and Savage [1986] and sin which tend to the correct limit at closest packing.

The KTGF models are choosed based on a sensitivity analysis where the Syamlal et al. model for the granular viscosity gave better results and were more stable, along with sin model for the radial function.

When the solid phase fraction is high in a particular zone of the domain, lots of contacts among particles occur and a frictional stress derives from them that must be accounted for in the mathematical model. In this state the collisions among particles could not be considered instantaneous as previously done in the kinetic theory and the frictional stress is accounted for adding a term in the granular pressure and in the granular viscosity. Hence, the solid shear viscosity μ_S is expressed by Eq.(3.12):

$$\begin{aligned} \mathcal{P}_{\mathfrak{s}} &= \mathcal{P}_{\text{kinetic}} + \mathcal{P}_{\mathfrak{s},\mathfrak{fr}} \\ \mu_{\mathfrak{s}} &= \mu_{\text{kinetic}} + \mu_{\mathfrak{s},\mathfrak{fr}} \end{aligned} \tag{3.12}$$

$$\mathcal{P}_{\mathfrak{s},\mathfrak{fr}} = \mathcal{F}\mathfrak{r}\frac{(\alpha_{\mathfrak{s}} - \min(\alpha_{\mathfrak{s}}))^{\mathfrak{n}}}{(\alpha_{\mathfrak{s},\max} - \alpha_{\mathfrak{s}})^{\mathfrak{p}}} \tag{3.13}$$

where $\mathcal{F}\mathfrak{r} = 0.05$, $\mathfrak{n} = 2$ and $\mathfrak{p} = 5$ are empirical constants. The frictional shear viscosity is than expressed by:

$$\mu_{\mathfrak{s},\mathfrak{fr}} = \mathcal{P}_{\mathfrak{s},\mathfrak{fr}} \sin\delta \tag{3.14}$$

being δ the angle of internal friction of the particle.

NB: The frictional stress is added to the stress predicted by the kinetic theory when the solids volume fraction exceeds a critical value. This value is normally set to 0.5 when the flow is three-dimensional and the maximum packing limit is about 0.63.

3.2 Pressure drop calculations for single phase flow

The single-phase flow simulations are carried out to validate the modeling approach, the choice of the turbulence model as well as various essential parameters in order to carry out the treatment of the area near the wall. Also to validate the surrogates models approach. The pressure drop data for different water flow rates is recorded for cases of : horizontal pipe, inclined pipe and pipe with elbow. The results of the CFD code are compared with predicted values from theoretical correlations found in the literature. Table 3.2 shows different correlations to calculate the pressure drop for each setup.

Table 3.2: Pressure drop correlations

Correlations	Pipe Set up
$\Delta\mathcal{P}_{\mathfrak{f}} = -\mathfrak{f}\frac{\rho_{\mathfrak{W}}\mathrm{L}}{\mathrm{D}}\frac{\mathrm{U}_{\mathfrak{W}}{}^{2}}{2}$	Horizontal Pipe
$\Delta\mathcal{P} = -\Delta\mathcal{P}_{\mathfrak{f}} - \rho_{\mathfrak{W}}\mathfrak{g}\mathfrak{L}\sin(\theta)$	Inclined Pipe
$\Delta\mathcal{P} = -\Delta\mathcal{P}_{\mathfrak{f}} - \rho_{\mathfrak{W}}\mathfrak{g}\mathfrak{L}_{\mathrm{inclined}}\sin(\theta) - \mathcal{K}_{\mathfrak{L}}\frac{\rho\mathcal{U}_{\mathfrak{W}}^{2}}{2}$	Pipe with Bend

The implicit relation proposed by Colebrook, Eq.(3.15), is used to calculate the friction factor for turbulent flows in rough pipes.

$$\frac{1}{\sqrt{f}} = -2\log\left(\frac{e}{3.71D} + \frac{2.51}{\mathrm{Re}\sqrt{f}}\right) \tag{3.15}$$

where $\frac{e}{D}$ is the relative roughness, and is related the pipe material properties.

3.3 Turbulence model

The turbulence aspect must be ensured when transporting a slurry. Since, this will guarantee the pseudo-homogeneity of the mixture and will subsequently prevent total sedimentation of the solid phase. In this work, the flow is characterized by a Reynolds number of order of 10^6. This is why the turbulence of water for both single or two phase flow is treated with the standard k-ϵ model, which is a high Reynolds turbulence model. However, wall functions are used to treat the boundary-layer development up to the wall. Eq.(3.16) and Eq.(3.17) present the model variables, the turbulent kinetic energy k and the turbulence dissipation rate ϵ respectively:

$$\frac{\partial(\rho_W k_W)}{\partial t} + \frac{\partial(\rho_W k_W U_{W_i})}{\partial x_i} = \frac{\partial}{\partial x_j}\left[\left(\mu_W + \frac{\mu_t}{\sigma_k}\right)\frac{\partial k_W}{\partial x_j}\right] + G_k + G_b - \rho_W \varepsilon_W + S_k \tag{3.16}$$

$$\frac{\partial(\rho_W \varepsilon_W)}{\partial t} + \frac{\partial(\rho_W \varepsilon_W U_{W_i})}{\partial x_i} = \frac{\partial}{\partial x_j}\left[\left(\mu + \frac{\mu_t}{\sigma_\varepsilon}\right)\frac{\partial \varepsilon_W}{\partial x_j}\right] + \frac{C_{1\varepsilon}\varepsilon_W}{k_W}(G_k + C_{3\varepsilon}G_b) - C_{2\varepsilon}\rho\frac{\varepsilon_W^2}{k_W} + S_\varepsilon \tag{3.17}$$

3.4 Near-wall treatment

The near-wall treatment is done using the wall functions method. The wall functions consist of wall boundary conditions that impose values for the kinetic energy k_P and the dissipation rate ϵ_P in the center of the cells near the wall as shown by Eq.(3.18) and Eq.(3.19), which bridges turbulent quantities on the wall.

$$k_P = \frac{\sqrt{f U_W^2}}{\sqrt{2C\mu}} \tag{3.18}$$

$$\epsilon_P = \frac{C_\mu^{3/4} K_P^{3/2}}{k\ y_P} \tag{3.19}$$

$C_\mu = 0.09$ is a model coefficient of the $k-\epsilon$; $k = 0.41$ is Von Karman constant; y_P is the height to the center of the cell adjacent to the wall and it can be calculated from y^+ according to the Eq.(3.20).

$$y_p = \frac{y^+ \mu_W}{\rho_W \sqrt{f u_W}} \tag{3.20}$$

For the inlet turbulence conditions, Eq.(3.21) present the turbulent kinetic energy (k_{in}) that is obtained from the turbulence intensity (I) and the water inlet velocity (U_W) (Mes [d]):

$$k_{in} = \frac{3}{2} U_W^2 I^2 \tag{3.21}$$

Next, the length scale (l) of the turbulence at the inlet should be specified. For an internal pipe flow, this is usually $\sim 7\%$ of the pipe diameter. So the turbulent dissipation rate (ϵ_{in}) is calculated as shown in Eq.(3.22):

$$\epsilon_{in} = C_\mu \frac{k_{in}^{3/2}}{l} \tag{3.22}$$

Chapter 4

Methodology

After choosing the mathematical models necessary to simulate the diphasic flow, comes the part of the implementation under the CFD tool. In this work the open-source CFD toolbox openfoam was choosed to perform the simulations, considering its advantages by comparing it with other CFD tools. Figure 4.1 shows OpenFOAM software advantages.

The simulation workflow begins with the pre-processing where the geometry along with

		OpenFOAM	Commercial Software (ANSYS, STAR-CCM+ etc)
1.	Cost effectiveness	✓	✗
2.	Parallel computing	✓	✓
3.	Source code	✓	✗
4.	Redistribution of code	✓	✗
5.	Collaborative development	✓	✗
6.	Documentation	✗	✓
7.	GUI / user friendliness	✗	✓

Figure 4.1: Why OpenFOAM ?

the mesh are generated, after comes the part of choosing the solver which represent well our model, and then the post-processing where the results of the simulation are visualized. The twoPhaseEulerFoam solver is the one which represents well our model and the solver has been modified to become an isothermal flows solver, since there is no heat exchange between the phases. Then, in the constant file the different forces which act on the flow have been defined

according to the assumptions made, where thus the interphase momentum exchange models have been defined. Then the components of the KTGF are implemented taking into consideration the restitution coefficients. The implementation of the model also requires special attention to the boundary conditions which need a good understanding of the physical phenomenon to define them.

Bibliography

Numerical simulation of slurry flows in heterogeneous and saltation regimes in horizontal pipelines. 57.

a.

b.

a.

b.

c.

d.

Transport modeling of sedimenting particles in a turbulent pipe flow using euler–lagrange large eddy simulation. *International Journal of Multiphase Flow*, 75:1 – 11, 2015.

A. Akhtar, V. Pareek, and M. Tadé. Cfd simulations for continuous flow of bubbles through gas-liquid columns: Application of vof method. *Chemical Product and Process Modeling*, 2, 01 2007.

M. A. Al-Yaari and B. F. Abu-Sharkh. Cfd prediction of stratified oil-water flow in a horizontal pipe. *Asian Transactions on Engineering*, 1(5):68–75, 2011.

C. L. Antaya, K. F. K. Adane, and R. S. Sanders. Modelling concentrated slurry pipeline flows. 44755:1659–1671, 2012.

T. R. Auton, J. C. R. Hunt, and M. Prud'Homme. The force exerted on a body in inviscid unsteady non-uniform rotational flow. *Journal of Fluid Mechanics*, 197:241–257, 1988.

X. Bin and S. DaWen. Applications of computational fluid dynamics (CFD) in the food industry: a review. *Computers and Electronics in Agriculture*, 34, 2002.

B. M. Bossio, A. J. Blanco, and F. H. Hernandez. Eulerian-eulerian modeling of non-newtonian slurries flow in horizontal pipes. 43727:525–533, 2009.

L. Chen, Y. Duan, W. Pu, and C. Zhao. Cfd simulation of coal-water slurry flowing in horizontal pipelines. *Korean Journal of Chemical Engineering*, 26:1144–1154, 07 2009.

C. T. Crowe, J. D. Schwarzkopf, M. Sommerfeld, and Y. Tsuji. *Multiphase flows with droplets and particles*. CRC press, 2011.

D. A. Drew and S. L. Passman. *Theory of multicomponent fluids*, volume 135. Springer Science & Business Media, 2006.

J. Dufek and G. W. Bergantz. Suspended load and bed-load transport of particle-laden grav-

ity currents: the role of particle–bed interaction. *Theoretical and Computational Fluid Dynamics*, 21:119–145, 03 2007.

M. Elkarii, C. Bouallou, and A. Ratnani. Towards modelling a diphasic flow using the CFD technique to achieve a digital twin of a Phosphate slurry piping process. *Chemical Engineering Transactions*, 81:757–762, 2020.

M. K. Gopaliya and D. Kaushal. Modeling of sand-water slurry flow through horizontal pipe using cfd. *Journal of Hydrology and Hydromechanics*, 64(3):261 – 272, 2016.

F. H. Hernandez, A. J. Blanco, and L. Rojas-Solorzano. Cfd modeling of slurry flows in horizontal pipes. 48401:857–863, 2008.

L. Jing, C. Y. Kwok, Y. F. Leung, and Y. D. Sobral. Extended cfd-dem for free-surface flow with multi-size granules. *International Journal for Numerical and Analytical Methods in Geomechanics*, 40:62–79, 01 2016.

N. Kumar, M. K. Gopaliya, and D. Kaushal. Experimental investigations and cfd modeling for flow of highly concentrated iron ore slurry through horizontal pipeline. *Particulate Science and Technology*, 37(2):232–250, 2017.

S. Lahiri and K. Ghanta. Regime identification of slurry transport in pipelines: A novel modelling approach using ann & differential evolution. *Chemical Industry and Chemical Engineering Quarterly*, 16:329–343, 2010.

C. Lun and S. Savage. The effects of an impact velocity dependent coefficient of restitution on stresses developed by sheared granular materials. *Acta Mechanica*, 63(1-4):15–44, 1986.

C. Lun , S. Savage, D. Jeffrey, and N. Chepurniy . Kinetic theories for granular flow: Inelastic particles in couette flow and slightly inelastic particles in a general flowfield. *Journal of Fluid Mechanics*, 140:223 – 256, 03 1984.

M. R. Maxey and J. J. Riley. Equation of motion for a small rigid sphere in a nonuniform flow. *The Physics of Fluids*, 26(4):883–889, 1983.

T. N. Ofei and A. Y. Ismail. Eulerian-eulerian simulation of particle-liquid slurry flow in horizontal pipe. *Journal of Petroleum Engineering*, 2016:1–10, 2016.

T. N. Ofei, S. Irawan, and W. Pao. Cfd method for predicting annular pressure losses and

cuttings concentration in eccentric horizontal wells. *Journal of Petroleum Engineering*, 2014:1–16, 2014.

A. Passalacqua and R. O. Fox. Implementation of an iterative solution procedure for multi-fluid gas–particle flow models on unstructured grids. *Powder Technology*, 213(1-3):174–187, 2011.

A. Rabhi, A. Chkifa, S. Benjelloun, and A. Latifi. Surrogate-based modeling in flotation processes. *Computer Aided chemical engineering*, 43:229–234, 2018.

Y. Seong, C. Park, J. Choi, and I. Jang. Surrogate model with a deep neural network toevaluate gas–liquid flow in a horizontal pipe. *Energies*, 13:968, 2020.

M. K. Singh, S. Kumar, and D. Ratha. Computational analysis on disposal of coal slurry at high solid concentrations through slurry pipeline. *International Journal of Coal Preparation and Utilization*, 40(2):116–130, 2017.

M. Syamlal, W. Rogers, and T. J. O'Brien. Mfix documentation theory guide.

H. K. Versteeg and W. Malalasekera. An introduction to computational fluid dynamics: the finite volume method. 2007.

C. Y. Wen and Y. H. Yu. A generalized method for predicting the minimum fluidization velocity. *AIChE Journal*, 12(3):610–612, 1966.